Petroleum Science 23 (2026) 954–965

Contents lists available at ScienceDirect

Petroleum Science

journal homepage: www.keaipublishing.com/en/journals/petroleum-science

Original Paper

Long-term sustained release of small molecular surfactants using microcapsules

Shuang Liu [a], Ling-Ling Ren [a], Zheng Wang [a], Jia-Wei Shi [a], Chen-Guang Wang [a], Jia-Hui Guo [b], Lu Zhang [c], Hao-Ran Cheng [b], Li-Yuan Zhang [a,*]

[a] State Key Laboratory of Deep Oil and Gas, Shandong Key Laboratory of Oil and Gas Field Chemistry, School of Petroleum Engineering, China University of Petroleum (East China), Qingdao, 266580, Shandong, China
[b] College of Chemical Engineering, Qingdao University of Science and Technology, Qingdao, 266042, Shandong, China
[c] Key Laboratory of Photochemical Conversion and Optoelectronic Materials, Technical Institute of Physics and Chemistry, Chinese Academy of Sciences, Beijing, 100190, China

ARTICLE INFO

Article history:
Received 9 January 2025
Received in revised form
20 August 2025
Accepted 6 November 2025
Available online 13 November 2025

Edited by Min Li

Keywords:
Microfluidics
Microcapsule
Sustained release
Small molecular surfactant
Encapsulation

ABSTRACT

The controlled manipulation of surfactant concentration is essential for optimizing performance in numerous industrial applications, such as enhanced oil recovery in oil industry. However, encapsulating surfactants has proven challenging due to their propensity to localize at interfaces. In this study, we use microfluidic technology to fabricate poly (ethylene glycol) diacrylate-based microcapsules for encapsulating small molecular cargoes through finely tuning the relationships among the interfacial tensions of inner, middle and outer phases. These microcapsules show excellent retention by regulating the shell thickness and monomer content, releasing less than 47.2% over 49 d at 20 °C. Upon oil contact, surfactant release is indicated by a contact angle decrease of 7.2° at 20 °C and 21.8° at 50 °C within 48 h. The releases of nonionic Tween 80 and zwitterionic Betaine 1 calculated via surface tension in saline solutions at 80 °C are reduced to as low as 8.2% within 48 h and 1.1% within 8 h. The pressure-induced release reaches 22.7% within 24 h under 15 MPa, significantly exceeding the impacts of temperature and salinity. Notably, even microcapsules with reduced eccentricity still demonstrate sustained-release behavior. Mechanical and degradation tests show that the sustained release is driven by the increase in pore size of the shell due to its gradual degradation. This tunable system offers a versatile platform for encapsulating and controlling the release of surfactants or other sensitive agents, ideal for harsh environmental applications requiring sustained functionality.

1. Introduction

The controlled release of surfactants from encapsulated carriers is essential for modulating local surfactant concentrations in microenvironments (Bergfreund et al., 2021; Liang et al., 2022), which has a broad application in drug delivery (Alemi et al., 2018; Boucard et al., 2018) and enhanced oil recovery areas (Liu et al., 2021; Razzaghi-Koolaee et al., 2022; Manshad et al., 2024). Encapsulating surfactants in a micron- or nano-sized carrier followed by releasing them in a controlled manner would be a great way to finely tune interfacial property (Fang et al., 2019; Bahraminejad et al., 2022). Moreover, releasing surfactants over a long period greatly reduces overall consumption (Hammami et al., 2023), improves efficiency (Alsmaeil et al., 2021) and mitigates environmental side effects (Liang et al., 2024). However, encapsulating surfactants has been inherently difficult due to the nature of the surfactant molecules, therefore, preferring stay at the interfaces (Bahraminejad et al., 2021, 2024). Thus, increasing the solubility of surfactants in their interior phase and diminishing their tendency to the interface are essential to increase the encapsulation efficiency. The most common way to enhance surfactant solubility in bulk solutions is to introduce adjuvants (Jia et al., 2019; Zhang et al., 2024), such as additional surfactants (Chou et al., 2005), co-surfactants, and salts to reduce their interaction (Qazi et al., 2020; Gradzielski et al., 2021). However,

* Corresponding author.
E-mail address: liyuanzhang@upc.edu.cn (L.-Y. Zhang).
Peer review under the responsibility of China University of Petroleum (Beijing).

https://doi.org/10.1016/j.petsci.2025.11.019

this approach must consider compatibility between the adjuvants and the original substances, which is not suitable for all kinds of surfactants (Belhaj et al., 2020). Adjusting the pH or increasing ionic strength can alter the charge state of functional groups and the conformation of surfactant molecules, especially for non-ionic surfactant, therefore, increase the solubility in their interior phase (Bloor et al., 1970). Adding nanoparticles as surfactant carriers to reduce the contact probability between surfactant and the outer environment can retain more surfactants in the bulk solution (Alsmaeil et al., 2021). The challenging part lies in preparing stable and homogeneous nanoparticle suspension with high surfactant adsorption efficiency (Liu et al., 2021). Co-precipitation of surfactants with carrier polymers by forming nanoparticles allows for the encapsulation of surfactants within the particles (Dos Santos Francisco et al., 2023). Releasing surfactant can be challenging as the carrier polymer should be well suspended in the releasing environment, which narrows the choice of the carrier polymer (Guzmán et al., 2020; Zhou and Ranjith, 2022). Moreover, the encapsulation efficiency is relatively low due to the introduction of additional carrier materials (Romero-Zerón and Kittisrisawai, 2015; Gu et al., 2016; Constantin et al., 2017). Microcapsule with a thin tunable shell and a large cavity for loading concentrated surfactants is a promising carrier for delivering surfactant molecules (Li et al., 2018; Fang et al., 2019) and can be produced by chemical or physical approaches such as spray-based techniques (Chalella Mazzocato et al., 2019; Sun et al., 2020), physical encapsulation approaches such as coacervation (Ghorbani Gorji et al., 2018), layer-by-layer assembly (Jiang et al., 2022) and physical emulsification (Ma et al., 2020), chemical encapsulation strategies like interfacial polymerization (Duan et al., 2018), phase separation (Dowding et al., 2004) and solvent evaporation (Gu et al., 2016), and microfluidics (Nan et al., 2024). Nevertheless, conventional encapsulation methods frequently produce microcapsules exhibiting significant heterogeneity in both dimensional parameters and morphological organization, which severely limits the encapsulation efficiency (Sun et al., 2020) and releases rapidly (de Freitas et al., 2019). In contrast, microfluidic technique is of attraction for its ability of precisely control on fluid interfaces, reaction conditions and high throughput production of monodisperse multiphase emulsion droplets with tunable size, morphology and composition (Li et al., 2018; Ren et al., 2024). However, extra addition of active substances or amphiphilic molecules into the inner phase before generating double emulsion would disturb the interface, leading to the instability of the double emulsion template (Jiao et al., 2002) or cargo adsorption on the inner shell of microcapsules (Nam et al., 2018). Increasing the surfactant concentration in the inner phase without disturbing the interface is essential to successfully encapsulate surfactants in a double emulsion templated microcapsule. Cargo loaded particles can be released under diffusion (Huang et al., 2009), matrix swelling or degradation (Duncanson et al., 2012; Pei et al., 2019) and stimuli such as temperature (Lee et al., 2024), osmotic pressure (Seo et al., 2020), pH (Broaders et al., 2010) and magnetism (Wei et al., 2014). The release can be engineered to respond to chemical stimuli or physical stimuli through structural modifications (DiLauro et al., 2013), such as phase transition (Choi et al., 2021) and the porosity change of the capsule membrane (Pei et al., 2019). Silica-based nanosized porous capsules (MCM-41) have been confirmed to encapsulate cetyltrimethylammonium bromide (CTAB), enabling a slow, ion-triggered surfactant release of 46% over 12 d in saline environments (Alsmaeil et al., 2020). β-cyclodextrin was qualitatively verified as a novel sodium dodecyl sulfate (SDS) delivery system to release the surfactant hydrophobic tail (Alhassawi and Romero-Zerón, 2015). The temperature influence on the release is ambiguous. Therefore, it is challenging to fabricate a new surfactant encapsulation system with well-controlled release properties for fine-tuning the interfacial property.

In this work, we develop a small surfactant encapsulation system with a long-term release profile under extreme condition, as shown in Fig. 1. After optimization of a series of shell materials, we choose poly (ethylene glycol) diacrylate (PEGDA) as shell material. Moreover, due to the anti-adhesion property for active substances, the PEG membrane results in repulsive elastic forces when the active materials approach towards the substrate (Banerjee et al., 2011; Lee et al., 2005), which is suitable for confining the surfactants in the inner core of the double emulsion. We generate microcapsules that can encapsulate surfactant upon UV irradiation. The microcapsule structure can be controlled by varying the flow rate ratio and monomer concentration. These PEGDA microcapsules show excellent small molecular retention property, only releasing less than 20% in 49 d. Moreover, combining interfacial tension measurements, we directly obtain the release profile of ionic surfactant, Betaine 1 (ASB), which can not be measured through traditional UV spectrophotometer. We also study the release profile of these surfactant-laden microcapsules in brines with different concentrations at high temperatures and pressures. Moreover, we find that the release behavior of small molecules is mainly driven by pore size upon PEGDA shell degradation.

2. Materials and methods

2.1. Chemicals

The small molecular surfactants are Tween 80 (M_w = 1309) purchased from Biosharp and Betaine 1 (ASB) (M_w = 435) supported by China Petroleum Exploration and Development Research Institute. The polymers used include poly (vinyl alcohol) (PVA, Aladdin, China), poly (ethylene glycol) diacrylate (PEGDA, Sigma-Aldrich, USA), dextran T1 (M_w = 1000, Yuanye, China). Fluorescein sodium salt (Macklin, China), fluorescein isothiocyanate (Macklin, China) and calcein sodium salt (Macklin, China) are used for labelling microcapsules. Dichloromethane (DCM) (Macklin, China) serves as organic solvent in the middle phase. All reagents are used as received without further purification unless otherwise noted.

2.2. Fabrication of glass microfluidic device

The glass microfluidic device used for fabricating sustain-release microcapsules consists of two cylindrical glass capillaries (World Precision Instruments, Inc.). The glass capillaries are axis-aligned inserted into a square capillary (Harvard) from opposite directions. The assembly is then mounted on a glass slide using epoxy adhesive. Both cylindrical glass capillaries are tapered to achieve inner diameters of 30 and 250 μm. Finally, dispensing needles are positioned at the junctions, and secured onto the glass slide to form the emulsion droplets.

2.3. Fabrication of microcapsule

An aqueous 1 wt% PVA solution with fluorescein sodium salt serve as the inner aqueous phase. DCM containing 1 wt% photo-initiator and PEGDA with various concentrations of 10–30 wt% are used as middle oil phase. An aqueous solution of 5 wt% PVA acts as the outer phase. All phases are injected at constant flow rates using pumps (LSP01-3A, Longerpump). UV-polymerization of the shell is initiated within the device immediately after the formation of the template double emulsion droplets.

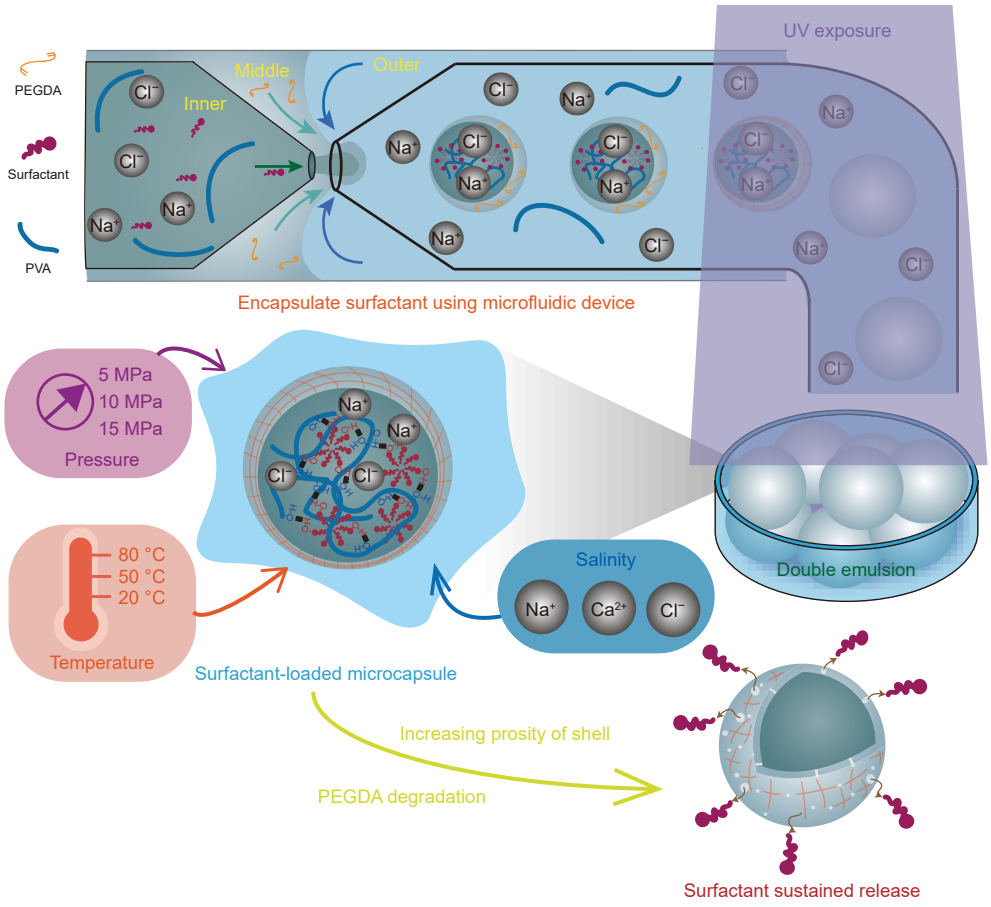

Fig. 1. Schematic illustration of microcapsule fabrication and surfactant release from PEGDA microcapsules.

2.4. Quantification of release profile for PEGDA microcapsules

The fluorescein sodium salt release in each microcapsule sample is measured using an ultraviolet–visible spectrophotometer (T6, Puxi) at room temperature. Three sets of microcapsule suspensions, with microcapsules collected for 30 min and suspended in ultrapure water (3.0 g), are prepared. The aqueous solution is then transferred to UV-VIS spectra and a calibration curve is obtained at the maximum absorbance peak of fluorescein sodium salt. This procedure is repeated three times with three different samples to reduce the error in the estimation of fluorescein sodium salt concentration and the standard deviation of absorbance values is less than 3%.

2.5. Preparation of Tween 80-loaded PEGDA microcapsules and ASB-loaded PEGDA microcapsules

We encapsulate Tween 80 (M_w = 1309) in PEGDA microcapsules using the same way as that for enwrapping fluorescein sodium salt. We dissolve 20 wt% PEGDA in DCM, supplemented with 1 wt% photoinitiator, serving as the middle phase. The inner phase is prepared as a solution containing 1 wt% PVA, 4 wt% Tween 80 with FITC-dextran. An aqueous solution of 5 wt% PVA acts as the outer phase. The washed microcapsules are placed in an outer phase at temperatures of 20, 50 and 80 °C. To investigate the effect of monovalent and divalent ions on the release rate of microcapsules, the washed microcapsules are placed in sodium chloride solutions (500, 1000, 2000 and 5000 mg·L^{-1}) and in calcium chloride solutions (600, 1200, 2400 and 6000 mg·L^{-1}). Additionally, other types of PEGDA microcapsule are cultured in NaCl solutions (3000, 5000 and 7000 mg·L^{-1}) and in $CaCl_2$ solutions (3000, 6000 and 9000 mg·L^{-1}) to further study the salt resistance of PEGDA shell.

The preparation of ASB-loaded microcapsules involves an inner phase composed of 1 wt% PVA, 1 wt% ASB with calcein sodium salt (M_w = 622.53 g·mol^{-1}). The middle phase consists of 20 wt% PEGDA and 1 wt% initiator in DCM, while the external phase is an aqueous solution of 5 wt% PVA.

2.6. Contact angle measurement

60 microcapsules are placed on a quartz sheet and inverted in simulated oil, mass ratio (toluene: *n*-decane) of 1:1. Ultrapure water (40 μL) is then added dropwise underwater, and the setup is maintained at temperatures of 20 and 50 °C to observe contact angle changes at the oil-water-solid three-phase interface. Contact angles were measured three times at each sampling point, ensuring a measurement uncertainty of less than 2°.

2.7. Surface tension measurement

We add microcapsules (0.1 g) to 0.5 wt% NaCl solution (10 g) and 0.6 wt% $CaCl_2$ solution (10 g) at temperatures of 20 and 80 °C. To investigate the effect of low salinity on the microcapsules, we add microcapsules to 0.3 wt% NaCl solution (10 g) and 0.3 wt% $CaCl_2$ solution (10 g) at 80 °C. The variation in surface tension is monitored over a period of 2 d.

2.8. The mechanical property of PEGDA shell

We mix PEGDA of 10, 15, 20, 25 and 30 wt%, and then pour the mixtures into the circular molds to expose under UV light. Subsequently, the slices with different monomer concentrations are placed in pure water at 20, 50 and 80 °C overnight. To simulate the harsh condition of high temperature and high salinity effect on the shell, we also culture the slices with 20 wt% PEGDA in 0.7 wt% NaCl solution and 0.9 wt% $CaCl_2$ solution at 80 °C for 12 h and 3 d. After immersion, the slices are washed with mass pure water, and then lyophilized to remove free water until the weight no longer changes. The mechanical properties of the PEGDA slices are measured using a rheometer (MCR 92, Anton Paar, Austria) with a parallel plate model. During the strain amplitude sweep tests, the shear strain (0.001%–100%) is fixed at an oscillation frequency (10 rad·s^{-1}). The relationship of pore size (ε) and storage modulus (G') is calculated by Eq. (1) (Rubinstein and Colby, 2003):

$$\varepsilon = \sqrt[3]{\frac{k_B T}{G'}} \tag{1}$$

where k_B is Boltzmann constant, T is Kelvin temperature, G' is storage modulus.

3. Results and discussion

3.1. Microfluidic fabrication of PEGDA microcapsule

Designing a carrier capable of stably encapsulating small-molecule surfactants requires overcoming a fundamental obstacle: these molecules inherently migrate to liquid-liquid interfaces (Zettlemoyer et al., 1967; Hosseinpour et al., 2021), which often destabilizes double emulsions prior to shell solidification. To address this, we begin with a systematic evaluation of potential shell materials, including PEGDA, styrene, polystyrene, and polystyrene-*b*-polyisoprene-*b*-polystyrene. PEGDA emerges as the optimal choice due to its anti-adhesive property, which stems from the hydrophilic PEG segments that generate repulsive elastic forces when active molecules approach the substrate (Lee et al., 2005; Banerjee et al., 2011). This feature makes PEGDA particularly well-suited for confining surfactants within the aqueous core of double emulsions (Fig. S1, Supplementary Information). To further enhance droplet stability before curing, we incorporate poly (vinyl alcohol) (PVA) into the inner aqueous phase. PVA, a hydrophilic polymer with polysaccharide-like characteristics, can form weak gels via intermolecular hydrogen bonding (Choi et al., 2021), thereby reducing interfacial adhesion (de Oliveira et al., 2014) and acting as a hydrophilic emulsifier. When blended with other surfactants, PVA improves droplet stability (Al-Sabagh, 2002). We test PVA at concentrations from 0 to 10 wt% and with different molecular weights, confirming its ability to stabilize microcapsules (Fig. S2, Supplementary Information). Microcapsules are fabricated using a coaxial glass capillary microfluidic device to generate stable W/O/W double emulsions (Fig. 2(a)). The immiscibility between the inner aqueous and organic middle phases ensures droplet stability, and immediate in-situ UV exposure initiates rapid PEGDA polymerization, forming a cross-linked shell around the inner phase (Fig. 2(b) and (c)). The resulting microcapsules have a mean diameter of 95.5 μm. Scanning electron microscopy of cross-sectioned capsules reveals a shell thickness ranging from 0.9 to 6.1 μm, indicating some degree of inhomogeneity across the shell structure (Fig. 2(d)).

3.2. Structure control of PEGDA microcapsules

The successful fabrication of surfactant laden microcapsules relies on forming stable emulsions before shell solidification. The stability of the W/O/W double emulsion before shell solidification depends on the ability of the middle oil phase to completely coat the inner aqueous phase. In a strict thermodynamic sense, the spreading coefficient for the middle oil phase (m) over the inner aqueous phase (i) is defined as:

$$S_{m/i} = \gamma_{i/o} - \left(\gamma_{m/o} + \gamma_{i/m}\right) \tag{2}$$

where $\gamma_{i/o}$ is the interfacial tension between the inner aqueous phase and the outer aqueous phase, $\gamma_{m/o}$ is the interfacial tension between the middle oil phase and the outer aqueous phase, $\gamma_{i/m}$ is the interfacial tension between the inner aqueous phase and the middle oil phase. A positive $S_{m/i}$ indicates that the oil phase will spontaneously spread over the inner aqueous phase, enabling double emulsion formation. In our system, the inner and outer phases are both aqueous and largely miscible, so $\gamma_{i/o}$ is effectively zero, making the strict thermodynamic formula impractical. This is a known limitation in double emulsion studies (Wang et al., 2013). To overcome this, we adopt an operational definition of S where $\gamma_{i/o}$ is replaced by the surface tension of the inner phase to air (γ_i), and $\gamma_{i/m}$ is approximated by the surface tension of the middle phase to air (γ_m). Although this approach is not a pure thermodynamic coefficient, it provides a useful comparative measure of wetting tendencies. Based on our measurements for Tween 80 encapsulation system: $\gamma_i = 35.0$ mN·m^{-1}, $\gamma_{m/o} = 2.7$ mN·m^{-1}, and $\gamma_m = 29.8$ mN·m^{-1}, yielding $S \approx 2.5$ mN·m^{-1}. This slightly positive value indicates that the middle oil phase can spread over the inner aqueous phase, supporting stable double emulsion formation prior to shell curing. A revised schematic (Fig. 3(a)) now shows only the three relevant phases and the measured interfacial/surface tensions, along with insets illustrating the difference between stable and collapsed emulsions. The double emulsion is successfully formed under kinetically driven microfluidic conditions. The combined effects of hydrodynamic focusing, interfacial stabilization by PVA, high PEGDA viscosity, and rapid UV polymerization allow for the formation of metastable double emulsions that are structurally stable and suitable for shell solidification.

We next explore how flow rates influence shell thickness. Keeping the total flow rate constant at 2000 μL·h^{-1} and the outer phase fixed at 8000 μL·h^{-1}, we vary the middle-to-inner phase flow rate ratio (Q_m/Q_i). Increasing Q_m/Q_i yields thicker shells, with a maximum thickness of 10.0 μm (Fig. 3(b)). Beyond this ratio, the emulsion becomes unstable. Monomer concentration also plays a decisive role. At a fixed flow rate, increasing PEGDA concentration from 10 to 30 wt% progressively thickens the shell from 7.3 to 14.5 μm (Fig. 3(c)) and enlarges the capsule diameter from 139.5 to 170.0 μm (Fig. 3(d)). When shell thickness is held constant at 5 μm, capsule diameter still increases with PEGDA concentration, ranging from 85.0 μm (10 wt%) to 136.6 μm (30 wt%). This behavior reflects the interplay between interfacial tension and shear stress (Zarzar et al., 2015; Wang et al., 2023, 2024), as well as the viscosity ratio between the continuous and dispersed phases (Fang et al., 2019). Higher-viscosity middle phases require smaller flow ratios to maintain the same shell thickness, inherently producing larger capsules. Collectively, these results confirm that the structural attributes of PEGDA microcapsules, shell thickness and overall size, can be precisely tuned by adjusting either the Q_m/Q_i ratio or the PEGDA monomer concentration, providing a controllable platform for optimizing encapsulation performance.

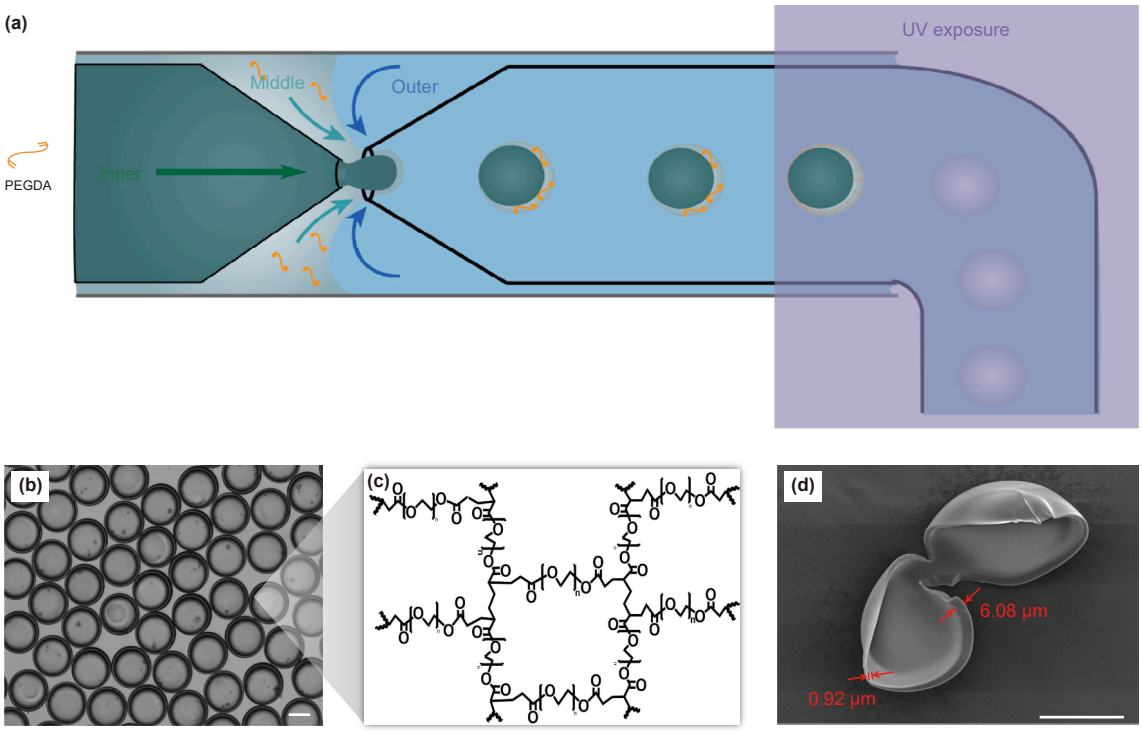

Fig. 2. Microfluidic fabrication of microcapsules. **(a)** Schematic illustration of microfluidic fabrication of microcapsules under UV exposure, **(b)** optical image of microcapsules, scale bar: 50 μm, **(c)** chemical structure of the polymerized PEGDA shell, **(d)** SEM image of PEGDA microcapsule, scale bar: 50 μm.

3.3. Release profile of fluorescein sodium salt from PEGDA-based microcapsule and surfactant-loaded PEGDA microcapsule

The release characteristics of small molecules from PEGDA microcapsules are strongly dictated by the properties of the polymer shell. To investigate this, we first encapsulate a model compound, fluorescein sodium salt, in microcapsules with a PEGDA shell concentration of 20 wt%. Over a 49-d observation period, most capsules preserve their spherical morphology, with only occasional localized swelling at structurally weaker points (Fig. 4(a)), indicating robust shell stability in aqueous environments. To examine how shell thickness influences release, we systematically vary it by adjusting the middle-to-inner phase flow rate ratio (Q_m/Q_i) while holding the total flow rate constant (2000 μL·h^{-1}; outer phase: 8000 μL·h^{-1}). Thinner shells (e.g., 3.1 μm at Q_m/Q_i = 2/3) release fluorescein sodium salt more rapidly, reaching a cumulative release of 47.2% after 49 d. Thicker shells (10.0 μm at Q_m/Q_i = 17/3) slow the release to 18.4% over the same period (Fig. 4(b)). Notably, no release curve plateaus during the study, even for the thinnest shells, underscoring the potential for long-term release applications (Zhang et al., 2019; Alsmaeil et al., 2021). However, capsules with pronounced eccentricity occasionally rupture at their thinnest regions, causing uncontrolled leakage (Fig. S3, Supplementary Information).

Release kinetics are analyzed using the Ritger-Peppas model (Losi et al., 2006), revealing diffusion exponents (n) greater than 0.5 under all conditions (Table S2, Supplementary Information).

$$Q = kt^n \tag{3}$$

where Q represents the fraction of the drug released, k is the kinetic constant accounting for the structural and geometric characteristics of the delivery system, t is the release time and n is the diffusion exponent. Thinner shells exhibit $0.5 < n < 1.0$, indicative of anomalous transport involving both diffusion and matrix erosion (Sinclair and Peppas, 1984), while thicker shells shift toward erosion-dominated release.

We next investigate the effect of PEGDA monomer concentration on release. With shell thicknesses ranging from 7.3 μm (10 wt%) to 14.5 μm (30 wt%), lower monomer concentrations produce faster release: after 36 d, cumulative release is 29.4 % for 10 wt% capsules and only 13.0% for 30 wt% capsules (Fig. 4(c)). When shell thickness is fixed at 5 μm, the trend persisted-cumulative release reaches 40.0 % for 10 wt% capsules versus 13.0 % for 30 wt% (Fig. 4(d)). These data fit well to the Higuchi model (Wójcik-Pastuszka et al., 2019), consistent with Fickian diffusion (Table S2):

$$Q = k_H t^{1/2} + k_1 \tag{4}$$

where Q is fraction of drug released, k_H is the Higuchi rate constant, t is the release time, k_1 is a constant.

To connect these findings to shell microstructure, we measure the mechanical properties of PEGDA slices polymerized at different monomer concentrations. Storage modulus (G') increases with concentration, while calculated pore size (ε) decreases (Fig. 4(e) and (f)). As monomer concentration increases, the material becomes denser, leading to a decrease in the pore size of the membrane material. This reduction in pore size enhances the spatial resistance for the cargo to escape through the pores, thereby significantly decreasing the release rate. Thus, the sustained release behavior observed at various monomer concentrations is attributed to the reduced release rate resulting from the smaller pore size.

Building on these insights, we encapsulate a functional nonionic surfactant, Tween 80, to evaluate interfacial performance. Capsules are placed at an oil-water-solid interface, and contact angles are monitored at 20 and 50 °C. At 20 °C, the contact

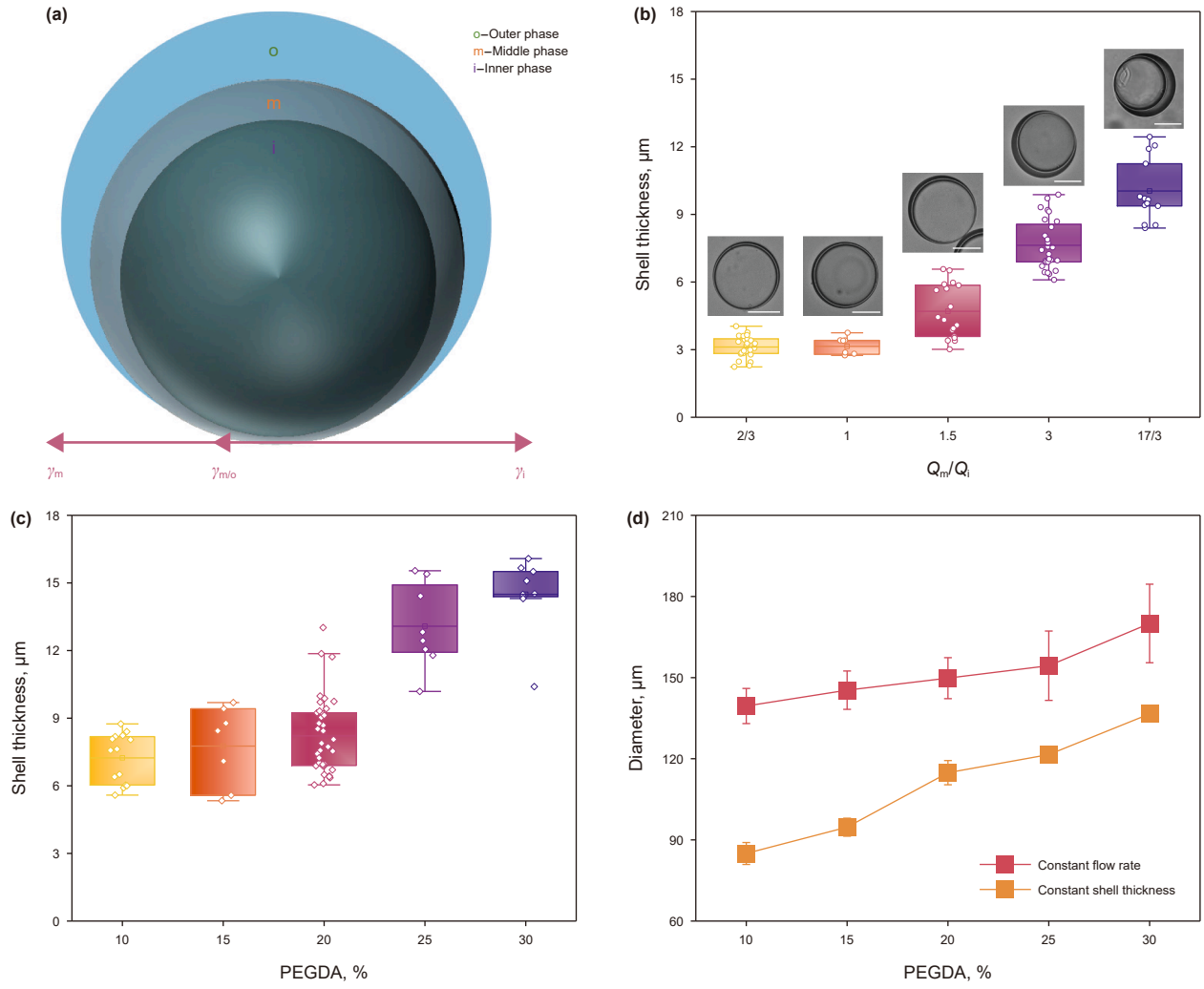

Fig. 3. The controllable structure of microcapsules. **(a)** Schematic illustration of the effect of interfacial tensions on the configuration of a complex droplet, **(b)** the effect of flow rate ratio (Q_m/Q_i) on shell thickness, scale bar: 50 μm, **(c)** variation in shell thickness with different PEGDA microcapsules under constant flow rates, **(d)** diameter of microcapsules as a function of PEGDA concentration, while maintaining constant flow rate or shell thickness. All standard deviations are listed in Table S1 (Supplementary Information).

angle decreases gradually from 30.2° to 23.0° over 48 h ($\Delta = -7.2°$), whereas at 50 °C the decrease is sharper, from 43.8° to 22.0° ($\Delta = -21.8°$) (Fig. 5(a) and (b)). This temperature-dependent reduction in contact angle confirms controlled release of Tween 80 from the capsules, with accelerated kinetics at elevated temperatures.

3.4. Thermal, salt and pressure resistance properties of microcapsule

To investigate the influence of temperature and salinity on the release profile, we encapsulate Tween 80 and FITC-dextran in PEGDA microcapsules (a mean diameter of 73.3 μm and shell thickness around 5.2 μm) (Fig. S4(a) and (b), Supplementary Information). The distinct green fluorescence emanating from the microcapsules is attributed to the encapsulated FITC-dextran. The microcapsules are homogeneous in size and intensity of the microcapsules. The microcapsules are incubated in 1000 mg·L^{-1} NaCl solution at 20, 50, and 80 °C, respectively. The fluorescence intensity gradually decreases over 24 h, as shown in Fig. 5(c)(i). The cumulative release profile reveals that after 24 h the release amount at 80 °C is up to 70.3%, larger than that of 9.3% at 20 °C, indicating that increasing temperature significantly accelerates the release rate, as observed in Fig. 5(c)(ii).

To study the effect of ions on the release profile, we also measure the release profiles of microcapsules in NaCl or $CaCl_2$ solution, ranging from 500 to 5000 mg·L^{-1}. The fluorescent intensity rapidly decreases under high salt concentrations over 24 h in Fig. 5(d)(i) and 5(e)(i). The microcapsules exhibit the slowest release rate in an isotonic salt solution, 9.3% in 1000 mg·L^{-1} NaCl solution or 8.8% in 1200 mg·L^{-1} $CaCl_2$ solution. In contrast, the most rapid release is observed in a hyperosmotic solution with a fivefold concentration of salt concentration, as revealed in Fig. 5(d)(ii) and 5(e)(ii). Moreover, the release profile has shown similar releasing trend under salt solution, implying that the release mechanism is predominantly governed by the osmotic pressure gradient instead of ion type.

To assess the capability of microcapsules under harsh conditions, we examine the release behavior of the microcapsules under various salinity solutions. The slowest release rates are observed in isotonic solutions, reaching 10.9% and 12.0% in 5000 mg·L^{-1} NaCl solution or 6000 mg·L^{-1} $CaCl_2$ solution after 24 h. The fastest release rates are found in high osmolarity solutions, reaching 88.8% and 88.2% in 7000 mg·L^{-1} NaCl solution and 9000 mg·L^{-1}

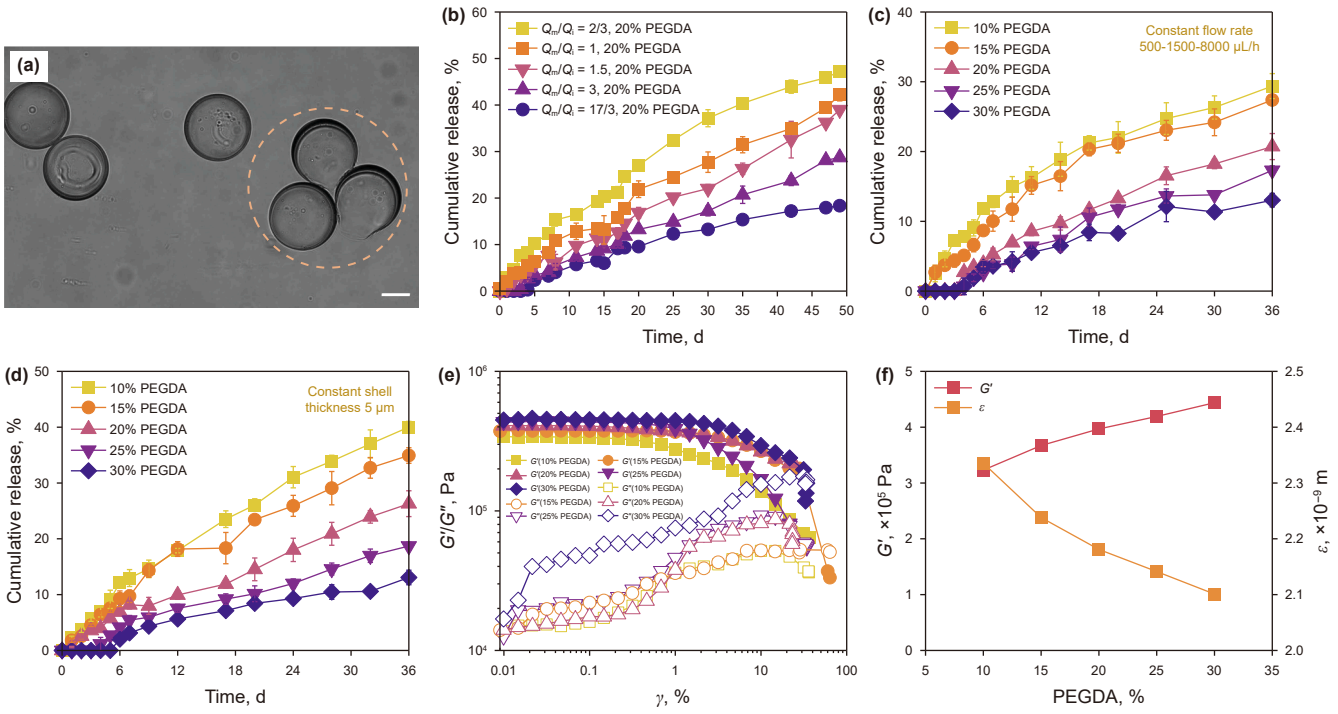

Fig. 4. Release profile of fluorescein sodium salt by PEGDA-based microcapsules. **(a)** Optical image of microcapsules after 49-d release, scale bar: 50 μm, **(b)** the cumulative release profile of fluorescein sodium salt in ultrapure water at different flow rate ratios ($n = 3$), **(c)** the cumulative release profile of fluorescein sodium salt as a function of shell monomer concentration ($n = 3$) in ultrapure water, **(d)** the cumulative release profile of fluorescein sodium salt as a function of shell monomer concentration with constant shell thickness ($n = 3$). All standard deviations are listed in Table S3 (Supplementary Information), **(e)** storage modulus (G') and loss modulus (G'') vs. strain for PEGDA slices with different concentrations, **(f)** the relationship of storage modulus (G'), pore size (ε) and PEGDA concentration.

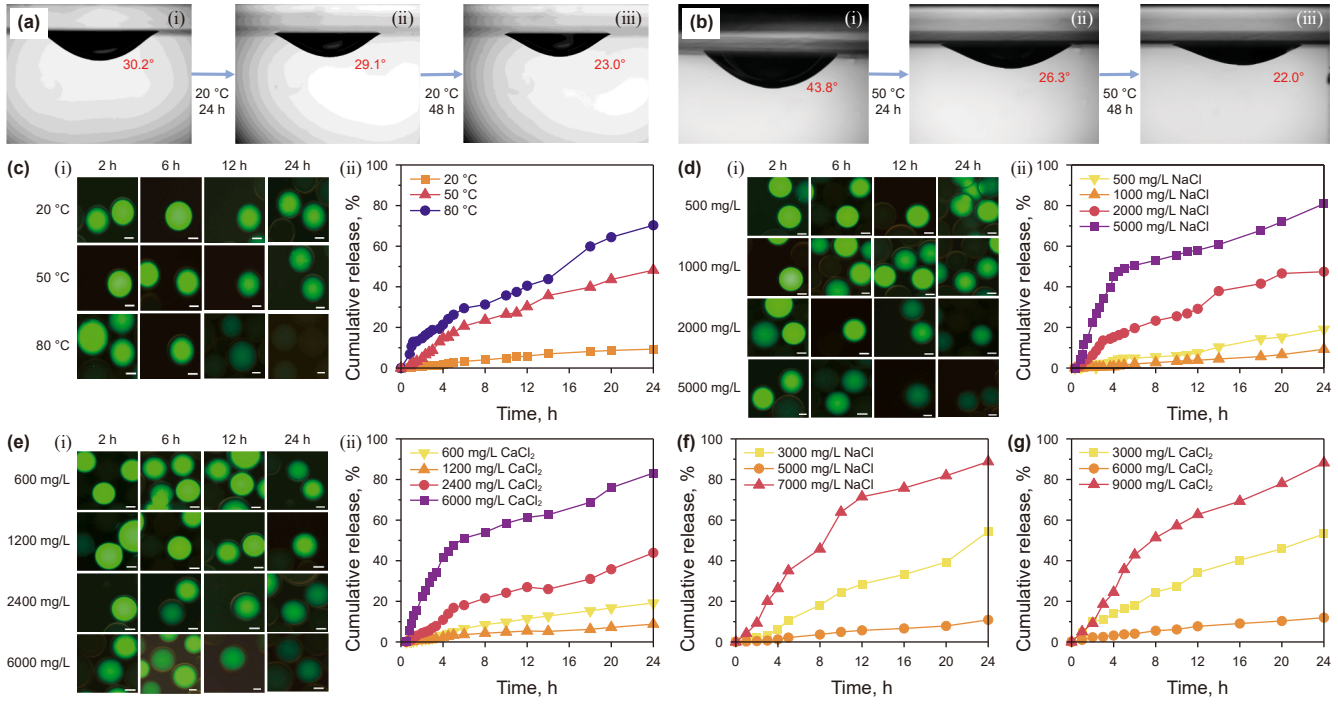

Fig. 5. Release behavior of Tween 80 indicated by FITC-dextran under harsh conditions. Photographs of contact angle variations after microcapsules contact simulated oil, **(a)** at 20 °C and **(b)** 50 °C for 48 h, respectively. (i) the initial moment; (ii) after 24 h; (iii) after 48 h. **(c)** (i) fluorescent images and (ii) cumulative release of Tween 80 released in 1000 mg·L^{-1} NaCl solution at 20, 50 and 80 °C, scale bar: 25 μm. **(d)** and **(e)** are fluorescent images (i) and cumulative release (ii) of Tween 80 released in NaCl and $CaCl_2$ solution, respectively, at 20 °C, scale bar: 25 μm. **(f)** and **(g)** are cumulative release of FITC-Dextran loaded microcapsules in NaCl and $CaCl_2$ solutions, respectively, at 20 °C.

$CaCl_2$ solution, respectively, after 24 h (Fig. 5(f) and (g)). Moreover, the cumulative concentration under high salinity solutions is similar to those under low salinity solutions. These results prove that our microcapsules have high salt resistance, and still possess a sustained release profile in the harsh conditions.

The cumulative concentration for fluorescent dye is reaching more than 12% over 24 h, which is much higher than 0.6% which we have measured in deionized water. The possible reason might be caused by the instability of the dye under harsh conditions, such as high temperatures and high salt concentrations (Liu et al., 2005). Moreover, some industrial-grade products might not be able to get fluorescent intensity, therefore, can not determine the release profile. Thus, we develop a new approach to characterize the concentration of the released surfactant. We have plotted the surface tension as a function of surfactant concentration, which is the "standard curve" for each surfactant. After measuring the surface tension for each time point, we can directly calculate the concentration from the standard curve. The micelle concentration (CMC) for Tween 80, 0.0000132 mol·L^{-1}, is shown in Fig. 6(a). We prepare Tween 80-loaded microcapsules and measure the surface tension of the solutions by dispersions of 0.1 g of microcapsules in 10 g of NaCl or $CaCl_2$ solution within 48 h, as shown in Fig. S5 (Supplementary Information). The surface tension diminishes from 61.6 to 47.9 mN·m^{-1} in 0.5 wt% NaCl solution and 49.8 mN·m^{-1} in 0.6 wt% $CaCl_2$ solution within 48 h. Conversely, at 80 °C, the reduction in surface tension is markedly rapid, plummeting to below 40 mN·m^{-1} within 48 h. Furthermore, in a low osmolarity brine solution at 80 °C, the release of the surfactant is quite fast during the initial 4 h, with no significant difference observed compared to the isotonic release after the 4 h, as illustrated in Fig. 6(b). Following a 48-h release period at 20 °C, Tween 80 exhibits a release of 1.3% in an isotonic sodium chloride solution and 0.8% in an isotonic calcium chloride solution. The release rate significantly increases at 80 °C, with release percentages of 8.2% and 9.0% observed in isotonic solutions, respectively. In low osmolality solution, the release rates increase to 13.7% and 17.6%, respectively, after 48 h, as illustrated in Fig. 6(c).

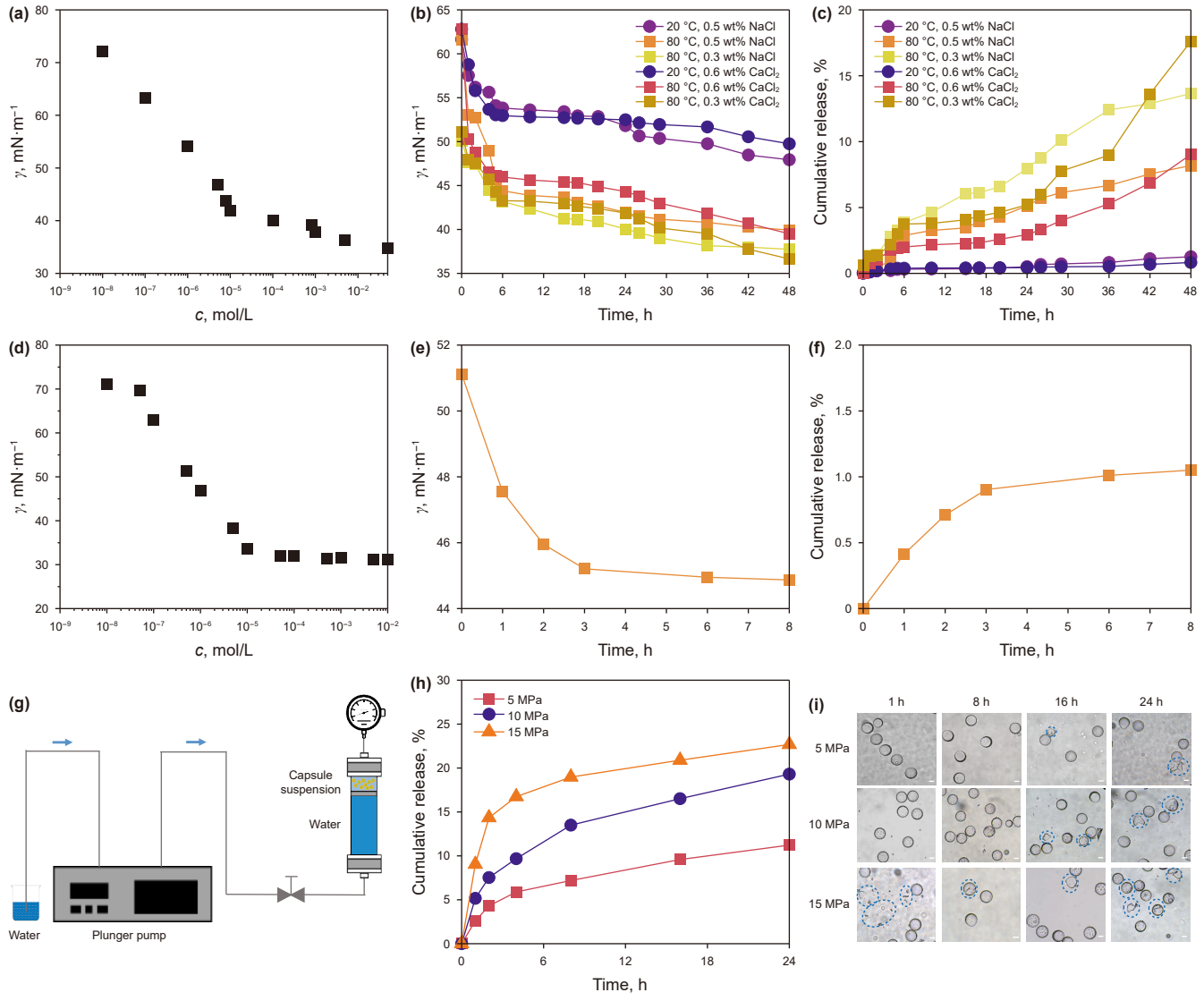

Fig. 6. Release profiles of Tween 80 and ASB under harsh condition. **(a)** Surface tension of Tween 80 at different concentrations, **(b)** surface tension and **(c)** cumulative release of Tween 80-loaded microcapsule suspension in different brines at 20 or 80 °C, **(d)** surface tension of ASB at different concentrations, **(e)** surface tension and **(f)** cumulative ASB release of ASB-loaded microcapsule suspension in NaCl solution at 80 °C, **(g)** schematic illustration of the pressurized microcapsule release apparatus, **(h)** the release profiles of microcapsules under pressures of 5, 10 and 15 MPa at 25 °C, **(i)** optical images of microcapsules subjected to pressure at various time intervals, scale bar: 25 μm.

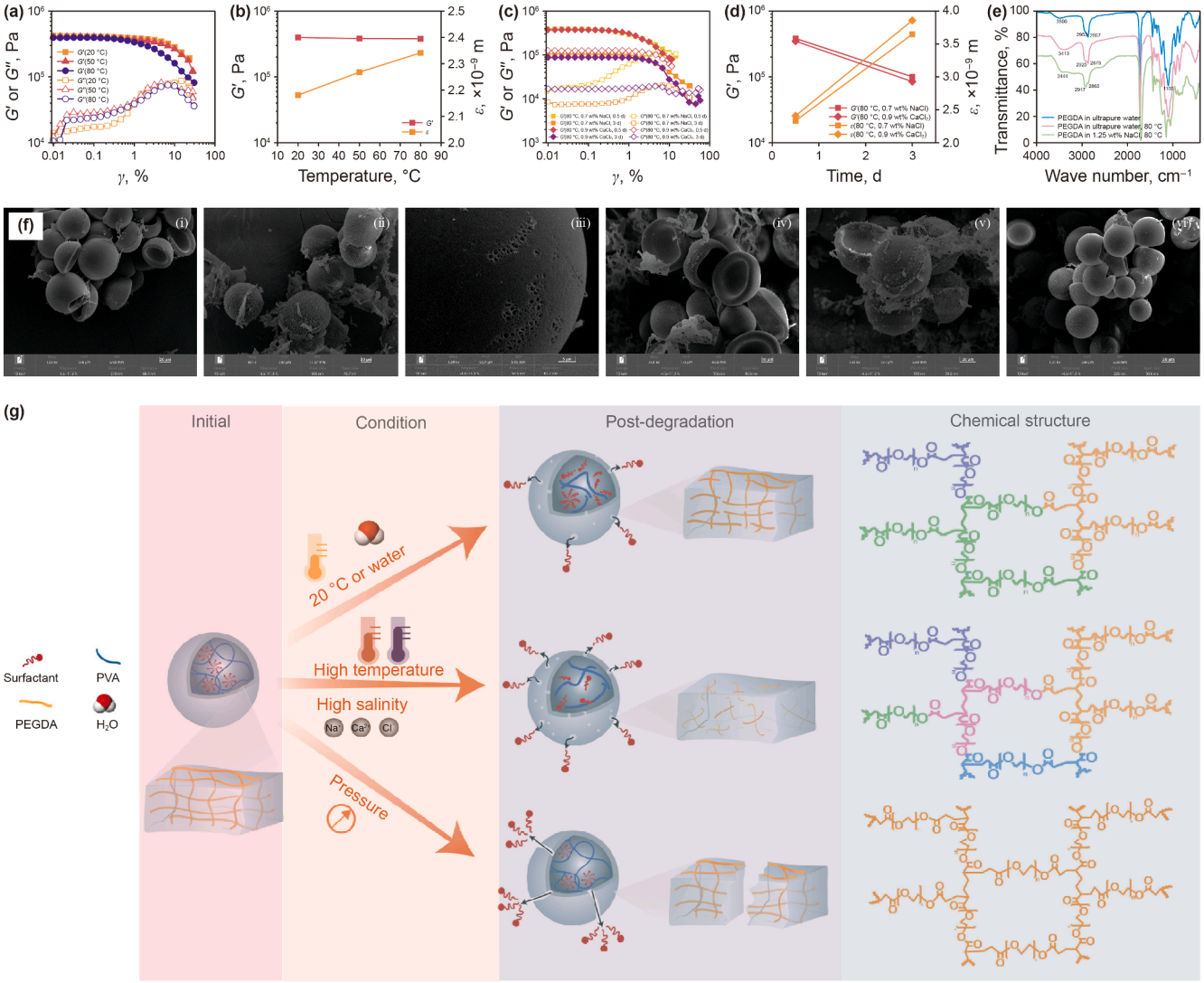

Fig. 7. Sustained release mechanism of PEGDA microcapsules. **(a)** Shell mechanical property of 20 wt% PEGDA slices in ultrapure water for 1 d at 20, 50 and 80 °C, **(b)** storage modulus (G') and pore size (ε) of PEGDA hydrogel vs. temperature, **(c)** shell mechanical property of 20 wt% PEGDA slices immersing in brines over time at 80 °C, **(d)** storage modulus (G') and pore size (ε) of PEGDA hydrogel vs. time at 80 °C in 0.7 wt% NaCl solution and 0.9 wt% $CaCl_2$ solution, **(e)** FTIR spectrum of PEGDA capsules, **(f)** SEM images of degraded microcapsules in (i) ultrapure water at 80 °C for 14 d; (ii) and (iii) 1.25% NaCl solution at 80 °C after 7 d; (iv) NaCl solution after 24 h under 5 MPa; (v) NaCl solution after 24 h under 10 MPa; (vi) NaCl solution after 24 h under 15 MPa, **(g)** schematic diagram of sustained release mechanism of PEGDA microcapsule.

To substantiate the versatility of our encapsulation method for surfactants, we extend our investigations to the industrial product, ASB, a zwitterionic surfactant. We apply the same approach to get the standard curve of ASB (CMC = 0.00001 mol·L^{-1}), as shown in Fig. 6(d). Due to the smaller molecule of ASB, the release rate is higher than Tween 80. Therefore, we only conduct a short period experiment up to 8 h. After release, the surface tension decreases to 44.9 mN·m^{-1} (Fig. 6(e)), with a cumulative release of 1.1% at 80 °C (Fig. 6(f)) following a first order model (Wójcik-Pastuszka et al., 2019) (Table S4, Supplementary Information):

$$Q = k_2\left(1 - e^{k_3 t}\right) \tag{5}$$

where Q is fraction of drug released, k_2 is a kinetic constant, k_3 is the first order rate constant, t is release time. Our results indicate the successful encapsulation and sustained release of surfactants, including the ionic surfactant. The release concentrations of surfactants at various future time points can be approximately predicted using the fitting release models.

To assess mechanical robustness, Tween 80 loaded capsules are subjected to 5, 10, and 15 MPa in hypotonic brine using the setup in Fig. 6(g). Release increases with pressure, reaching 11.2%, 19.3%, and 22.7% after 24 h, respectively (Fig. 6(h)). All groups exhibit an initial burst within 2 h, with shorter burst durations at higher pressures. Morphological analysis shows most capsules remain intact at ≤10 MPa, though eccentric capsules occasionally rupture. At 15 MPa, partial ruptures are more frequent, yet the majority of capsules retain structural integrity (Fig. 6(i)). Together, these results demonstrate that PEGDA microcapsules can withstand high temperature, high salinity, and elevated pressure, maintaining controlled release kinetics even under the challenging conditions relevant to subsurface applications.

3.5. *Release control strategies and influencing factors in microcapsule system*

The sustained release behavior of PEGDA microcapsules results from a combination of physical diffusion and structure-dependent

degradation mechanisms. These processes are governed by intrinsic material properties of the PEGDA network and by external environmental factors such as temperature, salinity, and pressure. Understanding how these variables influence shell integrity and pore evolution is critical for the rational design of release systems (Zhao, 2013). To investigate the influence of temperature on the hydrogel shell, we immerse PEGDA (20 wt%) cylindrical slices in ultrapure water at 20, 50, and 80 °C for 24 h. Rheological measurements show that the storage modulus (G') remains relatively stable, with values of 3.97×10^5, 3.82×10^5 and 3.80×10^5 Pa (Fig. 7(a)), respectively. The calculated pore sizes slightly increase with temperature, from approximately 2.2 to 2.5 nm (Fig. 7(b)), indicating that pure thermal stress induces minimal softening of the polymer matrix. This finding aligns with the modest enhancement in surfactant release observed at elevated temperatures. Salinity exerts a stronger impact on shell integrity. When slices are incubated in 0.7 wt% NaCl or 0.9 wt% $CaCl_2$ at 80 °C, the storage modulus declines significantly after 3 d, reaching 10^5 and 8.5×10^4 Pa, respectively (Fig. 7(c)). Corresponding pore sizes increase to 3.6 and 3.9 nm, as shown in Fig. 7(d) and Fig. S6 (Supplementary Information). Gravimetric analysis confirms hydrogel degradation, with mass loss ratios increasing from 3% at 0.5 d to over 5% at 3 d (Table S5, Supplementary Information). These results indicate that high salinity accelerates hydrolysis of the PEGDA network, facilitating cargo diffusion by enlarging the pore structure.

Fourier-transform infrared spectroscopy (FTIR) verifies chemical changes in the polymer matrix in Fig. 7(e). After exposure to 80 °C and high-salinity environments, a broad absorption band appears at 3400–3500 cm^{-1}, corresponding to hydroxyl group formation due to ester bond cleavage. The C–O–C stretching vibration at 1100 cm^{-1} decreases in intensity, indicating backbone scission (Bahraminejad et al., 2019). These spectroscopic changes support PEGDA degradation via hydrolysis of acrylate ester groups (Browning and Cosgriff-Hernandez, 2012; Browning et al., 2014; Parlato et al., 2014; Rodriguez-Rivera et al., 2024).

We use SEM imaging to correlate mechanical weakening with morphological changes. Capsules incubated in ultrapure water at 80 °C retain smooth, intact surfaces shown in Fig. 7(f)(i)), while those stored in 1.25 wt% NaCl exhibit cracking and salt deposition (Fig. 7(f)(ii)), indicating osmotic stress and localized failure. Under mechanical pressure, the shells show progressive damage (Fig. 7(f)(iii)). Capsules maintain structural integrity at 5 MPa (Fig. 7(f)(iv)), appears surface fissures at 10 MPa (Fig. 7(f)(v)), and partial fragmentation occurs 15 MPa (Fig. 7(f)(vi)). These results highlight the sensitivity of capsule performance to mechanical load and structural heterogeneity. Taken together, these observations confirm that PEGDA microcapsules exhibit a coupled release mechanism: passive diffusion through nano-sized pores, and accelerated release through environmentally induced degradation (Fig. 7(g)). Temperature, salinity, and pressure collectively influence the crosslink density and porosity of polymer network, enabling sustained and tunable release even under harsh external conditions (Zhao, 2013).

4. Conclusion

In this study, we have successfully developed PEGDA-based microcapsules for the long-term, sustained release of small molecular surfactants, including nonionic surfactants (Tween 80) and zwitterionic surfactants (Betaine 1). By optimizing encapsulation parameters, we are able to enhance the concentration of surfactants in the microcapsule core and precisely control the release rate by adjusting the shell thickness and the monomer concentration. We have investigated the release profiles of these microcapsules under various harsh conditions, including varying temperatures, salinity levels, and applied pressures. The results show that temperature, salinity, and pressure all play significant roles in controlling the release rates of surfactants. Specifically, the release rate increases significantly with rising temperature, with the fastest release observed at 80 °C. Similarly, the release rate is higher in brine solutions with increased salinity, especially at higher salt concentrations. Pressure-induced release demonstrates a positive correlation, with higher pressures resulting in greater release rates. To ensure a fair comparison of these effects, we have standardized the experimental periods and conditions. Under consistent experimental timeframes (48 h for temperature and salinity experiments, and 24 h for pressure experiments), we observe that temperature has the most substantial effect on surfactant release, with a reduction in surface tension of up to 21.8% at 50 °C. Salinity influences the release rate, with higher salt concentrations accelerating the release, while pressure-induced release exhibits a burst effect, with the release reaching 22.7% under 15 MPa after 24 h. Our findings suggest that the sustained release behavior of PEGDA microcapsules is governed by a combination of temperature, salinity, and pressure, with each factor contributing differently to the overall release kinetics. By tuning these parameters, our system offers a versatile platform for controlled release applications, particularly in challenging environments such as oil reservoirs and other industrial settings.

CRediT authorship contribution statement

Shuang Liu: Writing – original draft, Visualization, Validation, Methodology, Investigation, Formal analysis, Data curation. **Ling-Ling Ren:** Supervision, Resources. **Zheng Wang:** Supervision, Resources, Methodology. **Jia-Wei Shi:** Methodology. **Chen-Guang Wang:** Resources, Methodology. **Jia-Hui Guo:** Resources, Methodology. **Lu Zhang:** Supervision, Methodology. **Hao-Ran Cheng:** Project administration. **Li-Yuan Zhang:** Writing – review & editing, Supervision, Resources, Project administration, Methodology, Funding acquisition, Conceptualization.

Declaration of interests

The authors declare that they have no known competing financial interests or personal relationships that could have appeared to influence the work reported in this paper.

Acknowledgements

The authors thank the National Natural Science Foundation of China Project (ZX20210340), National Talent Support Project (ZX20220351), Shandong Province Innovative Team and Talent Project (ZX20230148) and Research start-up funding projects of China University of Petroleum (East China) (20210085) for financial support. The support from the Department of Oil and Gas Field Chemistry, School of Petroleum Engineering, China University of Petroleum (East China) is also appreciated.

Appendix A. Supplementary data

Supplementary data to this article can be found online at https://doi.org/10.1016/j.petsci.2025.11.019.

References

Alemi, A., Zavar Reza, J., Haghiralsadat, F., Zarei Jaliani, H., Haghi Karamallah, M., Hosseini, S.A., Haghi Karamallah, S., 2018. Paclitaxel and curcumin coadministration in novel cationic PEGylated niosomal formulations exhibit enhanced

synergistic antitumor efficacy. J. Nanobiotechnol. 16, 28. https://doi.org/10.1186/s12951-018-0351-4.
Alhassawi, H., Romero-Zerón, L., 2015. New surfactant delivery system for controlling surfactant adsorption onto solid surfaces. Part I: static adsorption tests. Can. J. Chem. Eng. 93, 1188–1193. https://doi.org/10.1002/cjce.22217.
Al-Sabagh, A.M., 2002. The relevance HLB of surfactants on the stability of asphalt emulsion. Colloids Surf. A Physicochem. Eng. Asp. 204, 73–83. https://doi.org/10.1016/S0927-7757(01)01115-3.
Alsmaeil, A., Enotiadis, A., Hammami, M.A., Giannelis, E., 2020. Slow release of surfactant utilizing silica nanosized capsules. In: International Petroleum Technology Conference. https://doi.org/10.2523/IPTC-19754-MS.
Alsmaeil, A.W., Hammami, M.A., Enotiadis, A., Kanj, M.Y., Giannelis, E.P., 2021. Encapsulation of an anionic surfactant into hollow spherical nanosized capsules: size control, slow release, and potential use for enhanced oil recovery applications and environmental remediation. ACS Omega 6, 5689–5697. https://doi.org/10.1021/acsomega.0c06094.
Bahraminejad, H., Khaksar Manshad, A., Keshavarz, A., Iglauer, S., Mohammad Sajadi, S., 2024. Nanocomposite synergy for enhanced oil recovery: Macro and micro analysis of CeO_2/montmorillonite nanofluids in carbonate and sandstone reservoirs. Fuel 360, 130384. https://doi.org/10.1016/j.fuel.2023.130384.
Bahraminejad, H., Khaksar Manshad, A., Riazi, M., Ali, J.A., Sajadi, S.M., Keshavarz, A., 2019. CuO/TiO_2/PAM as a novel introduced hybrid agent for water—oil interfacial tension and wettability optimization in chemical enhanced oil recovery. Energy Fuel 33, 10547–10560. https://doi.org/10.1021/acs.energyfuels.9b02109.
Bahraminejad, H., Manshad, A.K., Iglauer, S., Keshavarz, A., 2022. NEOR mechanisms and performance analysis in carbonate/sandstone rock coated microfluidic systems. Fuel 309, 122327. https://doi.org/10.1016/j.fuel.2021.122327.
Bahraminejad, H., Manshad, A.K., Keshavarz, A., 2021. Characterization, micellization behavior, and performance of a novel surfactant derived from gundelia tournefortii plant during chemical enhanced oil recovery. Energy Fuel 35, 1259–1272. https://doi.org/10.1021/acs.energyfuels.0c03272.
Banerjee, I., Pangule, R.C., Kane, R.S., 2011. Antifouling coatings: recent developments in the design of surfaces that prevent fouling by proteins, bacteria, and marine organisms. Adv. Mater. 23, 690–718. https://doi.org/10.1002/adma.201001215.
Belhaj, A.F., Elraies, K.A., Mahmood, S.M., Zulkifli, N.N., Akbari, S., Hussien, O.S., 2020. The effect of surfactant concentration, salinity, temperature, and pH on surfactant adsorption for chemical enhanced oil recovery: a review. J. Pet. Explor. Prod. Technol. 10, 125–137. https://doi.org/10.1007/s13202-019-0685-y.
Bergfreund, J., Siegenthaler, S., Lutz-Bueno, V., Bertsch, P., Fischer, P., 2021. Surfactant adsorption to different fluid interfaces. Langmuir 37, 6722–6727. https://doi.org/10.1021/acs.langmuir.1c00668.
Bloor, J.R., Morrison, J.C., Rhodes, C.T., 1970. Effect of pH on the micellar properties of a nonionic surfactant. J. Pharmacol. Sci. 59, 387–391. https://doi.org/10.1002/jps.2600590325.
Boucard, J., Linot, C., Blondy, T., Nedellec, S., Hulin, P., Blanquart, C., Lartigue, L., Ishow, E., 2018. Small molecule-based fluorescent organic nanoassemblies with strong hydrogen bonding networks for fine tuning and monitoring drug delivery in cancer cells. Small 14, 1802307. https://doi.org/10.1002/smll.201802307.
Broaders, K.E., Pastine, S.J., Grandhe, S., Fréchet, J.M.J., 2010. Acid-degradable solid-walled microcapsules for pH-responsive burst-release drug delivery. Chem. Commun. 47, 665–667. https://doi.org/10.1039/C0CC04190D.
Browning, M.B., Cereceres, S.N., Luong, P.T., Cosgriff-Hernandez, E.M., 2014. Determination of the in vivo degradation mechanism of PEGDA hydrogels. J. Biomed. Mater. Res. 102, 4244–4251. https://doi.org/10.1002/jbm.a.35096.
Browning, M.B., Cosgriff-Hernandez, E., 2012. Development of a biostable replacement for PEGDA hydrogels. Biomacromolecules 13, 779–786. https://doi.org/10.1021/bm201707z.
Chalella Mazzocato, M., Thomazini, M., Favaro-Trindade, C.S., 2019. Improving stability of vitamin B12 (cyanocobalamin) using microencapsulation by spray chilling technique. Food Res. Int. 126, 108663. https://doi.org/10.1016/j.foodres.2019.108663.
Choi, Y.H., Hwang, J., Han, S.H., Lee, C., Jeon, S., Kim, S., 2021. Thermo-responsive microcapsules with tunable molecular permeability for controlled encapsulation and release. Adv. Funct. Mater. 31 (24), 2100782. https://doi.org/10.1002/adfm.202100782.
Chou, D.K., Krishnamurthy, R., Randolph, T.W., Carpenter, J.F., Manning, M.C., 2005. Effects of Tween 20® and Tween 80® on the stability of Albutropin during agitation. J. Pharmacol. Sci. 94, 1368–1381. https://doi.org/10.1002/jps.20365.
Constantin, M., Bucatariu, S.-M., Doroftei, F., Fundueanu, G., 2017. Smart composite materials based on chitosan microspheres embedded in thermosensitive hydrogel for controlled delivery of drugs. Carbohydr. Polym. 157, 493–502. https://doi.org/10.1016/j.carbpol.2016.10.022.
de Freitas, F.A., Keils, D., Lachter, E.R., Maia, C.E.B., Pais da Silva, M.I., Veiga Nascimento, R.S., 2019. Synthesis and evaluation of the potential of nonionic surfactants/mesoporous silica systems as nanocarriers for surfactant controlled release in enhanced oil recovery. Fuel 241, 1184–1194. https://doi.org/10.1016/j.fuel.2018.12.059.
de Oliveira, P.P.M., Bavaresco, V.P., Silveira-Filho, L.M., Schenka, A.A., Vilarinho, K.A. de S., Barbosa de Oliveira Severino, E.S., Petrucci, O., 2014. Use of a novel polyvinyl alcohol membrane as a pericardial substitute reduces adhesion formation and inflammatory response after cardiac reoperation. J. Thorac. Cardiovasc. Surg. 147, 1405–1410. https://doi.org/10.1016/j.jtcvs.2013.07.021.
DiLauro, A.M., Abbaspourrad, A., Weitz, D.A., Phillips, S.T., 2013. Stimuli-responsive core–shell microcapsules with tunable rates of release by using a depolymerizable poly(phthalaldehyde) membrane. Macromolecules 46, 3309–3313. https://doi.org/10.1021/ma400456p.
Dos Santos Francisco, A.D., Maia, K.C.B., Moura, J.G.V., Nascimento, R.S.V., Da Silva Lima, F., Grasseschi, D., 2023. Chitosan derivatives as surfactant carriers for enhanced oil recovery – experimental and molecular dynamic evaluations of polymer-surfactant interactions. Colloids Surf. A Physicochem. Eng. Asp. 671, 131644. https://doi.org/10.1016/j.colsurfa.2023.131644.
Dowding, P.J., Atkin, R., Vincent, B., Bouillot, P., 2004. Oil core–polymer shell microcapsules prepared by internal phase separation from emulsion droplets. I. Characterization and release rates for microcapsules with polystyrene shells. Langmuir 20, 11374–11379. https://doi.org/10.1021/la048561h.
Duan, G., Haase, M.F., Stebe, K.J., Lee, D., 2018. One-step generation of salt-responsive polyelectrolyte microcapsules via surfactant-organized nanoscale interfacial complexation in emulsions (SO NICE). Langmuir 34, 847–853. https://doi.org/10.1021/acs.langmuir.7b01526.
Duncanson, W.J., Zieringer, M., Wagner, O., Wilking, J.N., Abbaspourrad, A., Haag, R., Weitz, D.A., 2012. Microfluidic synthesis of monodisperse porous microspheres with size-tunable pores. Soft Matter 8, 10636–10640. https://doi.org/10.1039/C2SM25694K.
Fang, Z., Cao, X.R., Yu, Y.L., Li, M., 2019. Fabrication and characterization of microcapsule encapsulating EOR surfactants by microfluidic technique. Colloids Surf. A Physicochem. Eng. Asp. 570, 282–292. https://doi.org/10.1016/j.colsurfa.2019.02.045.
Ghorbani Gorji, E., Waheed, A., Ludwig, R., Toca-Herrera, J.L., Schleining, G., Ghorbani Gorji, S., 2018. Complex coacervation of milk proteins with sodium alginate. J. Agric. Food Chem. 66, 3210–3220. https://doi.org/10.1021/acs.jafc.7b03915.
Gradzielski, M., Duvail, M., de Molina, P.M., Simon, M., Talmon, Y., Zemb, T., 2021. Using microemulsions: formulation based on knowledge of their mesostructure. Chem. Rev. 121, 5671–5740. https://doi.org/10.1021/acs.chemrev.0c00812.
Gu, B., Sun, X., Papadimitrakopoulos, F., Burgess, D.J., 2016. Seeing is believing, PLGA microsphere degradation revealed in PLGA microsphere/PVA hydrogel composites. J. Contr. Release 228, 170–178. https://doi.org/10.1016/j.jconrel.2016.03.011.
Guzmán, E., Llamas, S., Fernández-Peña, L., Léonforte, F., Baghdadli, N., Cazeneuve, C., Ortega, F., Rubio, R.G., Luengo, G.S., 2020. Effect of a natural amphoteric surfactant in the bulk and adsorption behavior of polyelectrolyte-surfactant mixtures. Colloids Surf. A. Physicochem. Eng. Asp. 585, 124178. https://doi.org/10.1016/j.colsurfa.2019.124178.
Hammami, M.A., Kouloumpis, A., Qi, G., Alsmaeil, A.W., Aldakkan, B., Kanj, M.Y., Giannelis, E.P., 2023. Probing the mechanism of targeted delivery of molecular surfactants loaded into nanoparticles after their assembly at oil–water interfaces. ACS Appl. Mater. Interfaces 15, 6113–6122. https://doi.org/10.1021/acsami.2c18762.
Hosseinpour, S., Götz, V., Peukert, W., 2021. Effect of surfactants on the molecular structure of the buried oil/water interface. Angew. Chem. Int. Ed. 60, 25143–25150. https://doi.org/10.1002/anie.202110091.
Huang, K.S., Lu, K., Yeh, C.S., Chung, S.R., Lin, C.H., Yang, C.H., Dong, Y.S., 2009. Microfluidic controlling monodisperse microdroplet for 5-fluorouracil loaded genipin-gelatin microcapsules. J. Contr. Release 137, 15–19. https://doi.org/10.1016/j.jconrel.2009.02.019.
Jia, H., Lian, P., Leng, X., Han, Y., Wang, Q., Jia, K., Niu, X., Guo, M., Yan, H., Lv, K., 2019. Mechanism studies on the application of the mixed cationic/anionic surfactant systems to enhance oil recovery. Fuel 258, 116156. https://doi.org/10.1016/j.fuel.2019.116156.
Jiang, Z., Zhao, S., Yang, M., Song, M., Li, J., Zheng, J., 2022. Structurally stable sustained-release microcapsules stabilized by self-assembly of pectin-chitosan-collagen in aqueous two-phase system. Food Hydrocoll. 125, 107413. https://doi.org/10.1016/j.foodhyd.2021.107413.
Jiao, J., Rhodes, D.G., Burgess, D.J., 2002. Multiple emulsion stability: pressure balance and interfacial film strength. J. Colloid Interface Sci. 250, 444–450. https://doi.org/10.1006/jcis.2002.8365.
Lee, J.H., Choi, C., Lee, H., 2024. A universal strategy for microcapsule diversity via interfacial surfactant complexation in fluorocarbon oil-based triple emulsions. Adv. Funct. Mater., 2417921 https://doi.org/10.1002/adfm.202417921.
Lee, J.H., Go, A.K., Oh, S.H., Lee, K.E., Yuk, S.H., 2005. Tissue anti-adhesion potential of ibuprofen-loaded PLLA–PEG diblock copolymer films. Biomaterials 26, 671–678. https://doi.org/10.1016/j.biomaterials.2004.03.009.
Li, W., Zhang, L., Ge, X., Xu, B., Zhang, W., Qu, L., Choi, C.-H., Xu, J., Zhang, A., Lee, H., Weitz, D.A., 2018. Microfluidic fabrication of microparticles for biomedical applications. Chem. Soc. Rev. 47, 5646–5683. https://doi.org/10.1039/C7CS00263G.
Liang, W., Zhao, X., Wang, Xiaolei, Tang, Z., Zhang, X., Wang, Xia, 2024. Prediction of freshwater ecotoxicological hazardous concentrations of major surfactants using the QSAR–ICE–SSD method. Environ. Int. 185, 108472. https://doi.org/10.1016/j.envint.2024.108472.
Liang, X., Zhang, J., Li, M., Wang, K., Luo, G., 2022. Dynamic interfacial tension and adsorption kinetics of nonionic surfactants during microfluidic droplet formation process. Chem. Eng. J. 445, 136658. https://doi.org/10.1016/j.cej.2022.136658.
Liu, W.T., Wu, J.H., Li, E.S.Y., Selamat, E.S., 2005. Emission characteristics of fluorescent labels with respect to temperature changes and subsequent effects on

DNA microchip studies. Appl. Environ. Microbiol. 71, 6453–6457. https://doi.org/10.1128/AEM.71.10.6453-6457.2005.
Liu, Z., Zhao, G., Brewer, M., Lv, Q., Sudhölter, E.J.R., 2021. Comprehensive review on surfactant adsorption on mineral surfaces in chemical enhanced oil recovery. Adv. Colloid Interface Sci. 294, 102467. https://doi.org/10.1016/j.cis.2021.102467.
Losi, E., Bettini, R., Santi, P., Sonvico, F., Colombo, G., Lofthus, K., Colombo, P., Peppas, N.A., 2006. Assemblage of novel release modules for the development of adaptable drug delivery systems. J. Contr. Release 111, 212–218. https://doi.org/10.1016/j.jconrel.2005.12.006.
Ma, L., Shang, Y., Zhu, Y., Zhang, X., E, J., Zhao, L., Wang, J., 2020. Study on microencapsulation of lactobacillus plantarum LIP-1 by emulsification method. J. Food Process. Eng. 43, e13437. https://doi.org/10.1111/jfpe.13437.
Manshad, A.K., Mobaraki, M., Ali, J.A., Abdulrahman, A.F., Jaf, P.T., Bahraminejad, H., Akbari, M., 2024. Biphasic interfacial functioning improvement using naturally derived hop and dill surfactants in carbonate reservoirs. J. Environ. Chem. Eng. 12, 112365. https://doi.org/10.1016/j.jece.2024.112365.
Nam, C., Yoon, J., Ryu, S.A., Choi, C.-H., Lee, H., 2018. Water and oil insoluble PEGDA-based microcapsule: biocompatible and multicomponent encapsulation. ACS Appl. Mater. Interfaces 10, 40366–40371. https://doi.org/10.1021/acsami.8b16876.
Nan, L., Zhang, H., Weitz, D.A., Shum, H.C., 2024. Development and future of droplet microfluidics. Lab Chip 24, 1135–1153. https://doi.org/10.1039/D3LC00729D.
Parlato, M., Reichert, S., Barney, N., Murphy, W.L., 2014. Poly(ethylene glycol) hydrogels with adaptable mechanical and degradation properties for use in biomedical applications. Macromol. Biosci. 14, 687–698. https://doi.org/10.1002/mabi.201300418.
Pei, H., Abbaspourrad, A., Zhang, W., Wu, Z., Weitz, D.A., 2019. Water-triggered rapid release of biocide with enhanced antimicrobial activity in biodiesel. Macromol. Mater. Eng. 304. https://doi.org/10.1002/mame.201900156.
Qazi, M.J., Schlegel, S.J., Backus, E.H.G., Bonn, M., Bonn, D., Shahidzadeh, N., 2020. Dynamic surface tension of surfactants in the presence of high salt concentrations. Langmuir 36, 7956–7964. https://doi.org/10.1021/acs.langmuir.0c01211.
Razzaghi-Koolaee, F., Mehrabianfar, P., Soltani Soulgani, B., Esfandiarian, A., 2022. A comprehensive study on the application of a natural plant-based surfactant as a chemical enhanced oil recovery (CEOR) agent in the presence of different ions in carbonate reservoirs. J. Environ. Chem. Eng. 10, 108572. https://doi.org/10.1016/j.jece.2022.108572.
Ren, L., Liu, S., Zhong, J., Zhang, L., 2024. Revolutionizing targeting precision: microfluidics-enabled smart microcapsules for tailored delivery and controlled release. Lab Chip 24, 1367–1393. https://doi.org/10.1039/D3LC00835E.
Rodriguez-Rivera, G.J., Green, M., Shah, V., Leyendecker, K., Cosgriff-Hernandez, E., 2024. A user's guide to degradation testing of polyethylene glycol-based hydrogels: from in vitro to in vivo studies. J. Biomed. Mater. Res. 112, 1200–1212. https://doi.org/10.1002/jbm.a.37609.
Romero-Zerón, L.B., Kittisrisawai, S., 2015. Evaluation of a surfactant carrier for the effective propagation and target release of surfactants within porous media during enhanced oil recovery. Part I: dynamic adsorption study. Fuel 148, 238–245. https://doi.org/10.1016/j.fuel.2015.01.034.
Rubinstein, M., Colby, R.H., 2003. Polymer Physics. Oxford University Press. https://doi.org/10.1093/oso/9780198520597.001.0001.
Seo, H., Nam, C., Kim, E., Son, J., Lee, H., 2020. Aqueous two-phase system (ATPS)-based polymersomes for particle isolation and separation. ACS Appl. Mater. Interfaces 12, 55467–55475. https://doi.org/10.1021/acsami.0c16968.
Sinclair, G.W., Peppas, N.A., 1984. Analysis of non-fickian transport in polymers using simplified exponential expressions. J. Membr. Sci. 17, 329–331. https://doi.org/10.1016/S0376-7388(00)83223-8.
Sun, X., Cameron, R.G., Bai, J., 2020. Effect of spray-drying temperature on physicochemical, antioxidant and antimicrobial properties of pectin/sodium alginate microencapsulated carvacrol. Food Hydrocoll. 100, 105420. https://doi.org/10.1016/j.foodhyd.2019.105420.
Wang, S., Wang, H., Wu, Y., Cheng, Y., 2024. Numerical study of double emulsion generation in a flow-focusing microchannel by multiple-relaxation-time lattice boltzmann method. Phys. Fluids 36, 032010. https://doi.org/10.1063/5.0190747.
Wang, W., Li, B.Y., Zhang, M.J., Su, Y.Y., Pan, D.W., Liu, Z., Ju, X.J., Xie, R., Faraj, Y., Chu, L.Y., 2023. Microfluidic emulsification techniques for controllable emulsion production and functional microparticle synthesis. Chem. Eng. J. 452, 139277. https://doi.org/10.1016/j.cej.2022.139277.
Wang, W., Zhang, M.J., Xie, R., Ju, X.J., Yang, C., Mou, C.L., Weitz, D.A., Chu, L.Y., 2013. Hole–shell microparticles from controllably evolved double emulsions. Angew. Chem. Int. Ed. 52, 8084–8087. https://doi.org/10.1002/anie.201301590.
Wei, J., Ju, X.J., Zou, X.Y., Xie, R., Wang, W., Liu, Y.M., Chu, L.Y., 2014. Multi-stimuli-responsive microcapsules for adjustable controlled-release. Adv. Funct. Mater. 24, 3312–3323. https://doi.org/10.1002/adfm.201303844.
Wójcik-Pastuszka, D., Krzak, J., Macikowski, B., Berkowski, R., Osiński, B., Musiał, W., 2019. Evaluation of the release kinetics of a pharmacologically active substance from model intra-articular implants replacing the cruciate ligaments of the knee. Materials 12, 1202. https://doi.org/10.3390/ma12081202.
Zarzar, L.D., Sresht, V., Sletten, E.M., Kalow, J.A., Blankschtein, D., Swager, T.M., 2015. Dynamically reconfigurable complex emulsions via tunable interfacial tensions. Nature 518, 520–524. https://doi.org/10.1038/nature14168.
Zettlemoyer, A.C., Subba Rao, V.V., Fix, R.J., 1967. Rates of adsorption of wetting agents and detergents at 'graphon' solution interface. Nature 216, 683. https://doi.org/10.1038/216683a0.
Zhang, L., Hou, Q., Yan, K., Zheng, B., Wang, L., Wang, J., 2024. Surfactant foamulsion stability in the absence and presence of salt. J. Mol. Liq. 396, 123998. https://doi.org/10.1016/j.molliq.2024.123998.
Zhang, W., Qu, L., Pei, H., Qin, Z., Didier, J., Wu, Z., Bobe, F., Ingber, D.E., Weitz, D.A., 2019. Controllable fabrication of inhomogeneous microcapsules for triggered release by osmotic pressure. Small 15, 1903087. https://doi.org/10.1002/smll.201903087.
Zhao, C.X., 2013. Multiphase flow microfluidics for the production of single or multiple emulsions for drug delivery. Adv. Drug Deliv. Rev. 65, 1420–1446. https://doi.org/10.1016/j.addr.2013.05.009.
Zhou, J., Ranjith, P.G., 2022. Insights into interfacial behaviours of surfactant and polymer: a molecular dynamics simulation. J. Mol. Liq. 346, 117865. https://doi.org/10.1016/j.molliq.2021.117865.